

Stochastic Huygens and Partial Coherence Propagation through Thin Tissues

Scott A. Prahla^{a,b}, Donald D. Duncan^b, David G. Fischer^c

^a Oregon Medical Laser Center, Providence St. Vincent Medical Center, Portland, OR

^b Division of Biomedical Engineering, Oregon Health & Science University, Portland, OR

^c NASA Glenn Research Center, Cleveland, OH

ABSTRACT

Stochastic Huygens describes a method of propagating a partially coherent source by sampling the Huygens wavelets that evolve from each point of the wavefront. The amplitude and phase of each wavelet is tracked as the light passes through the optical system. We have previously described how a partially coherent wavefront may be simulated by propagating an ensemble of wavefronts with specified first and second-order statistics through simple optical systems. In this work we extend the modeling effort to include an ensemble of phase (or scattering) screens that characterize thin microscope tissue samples in the optical path.

Keywords: Partial Coherence, Diffraction, Henyey-Greenstein, Scatter Plate, Phase Plate

1. INTRODUCTION

We have used Monte Carlo techniques to approximate classic Huygen-Fresnel evolution of a field. Specifically, we have demonstrated the propagation of cylindrical, partially coherent light through free space¹ and through a lens system.^{2,3} Simulating changes in the spatial coherence of an optical field required both a method for evolving the field and a method for creating an ensemble of fields with a specified spatial coherence.⁴ To extend this formalism treat propagation through a thin layer of tissue, two additional problems must be solved: (1) two-dimensional fields must be propagated instead of the one-dimensional fields used for cylindrical propagation and (2) a method for the interaction of the field with the scattering tissue.

2. STOCHASTIC SIMULATION OF HUYGENS-FRESNEL WAVES

2.1 Definitions

The field U at a point is

$$U(x, y, z, t) = U(x, y, z) e^{i\omega t}$$

where the time dimension will be omitted. The axial direction is z and the transverse directions are x and y . The ensemble intensity $S(x, y, z)$ and the cross-spectral density $\mu(x_1, y, z; x_2, y, z)$ for a partially coherent field are^{5,6}

$$S(x, y, z) = \langle U(x, y, z)U^*(x, y, z) \rangle$$

and

$$\mu(x_1, y, z; x_2, y, z) = \frac{\langle U(x_1, y, z)U^*(x_2, y, z) \rangle}{\sqrt{S(x_1, y, z)}\sqrt{S(x_2, y, z)}}$$

where $U^*(x, y, z)$ is the complex conjugate of $U(x, y, z)$. The angle brackets denote ensemble averages over all field realizations. For convenience the source is located in the plane $z = 0$. In this paper, we will only use perfectly coherent source terms and consequently the ensemble averages disappear.

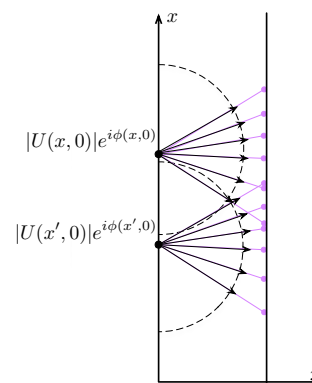


Figure 1. Rays used to approximate Huygen's wavelets.

Send correspondence to prahl@bme.ogi.edu, OMLC, PSVMC, 9205 SW Barnes Rd., Portland, OR 97225

The source field $U(x, y, 0)$ is evolved to the plane z by using a stochastic sampling technique. Each point in the source wavefront is considered to be the origin of a spherical wave (Huygens wavelet) emanating from that point. Each wavelet is uniformly sampled over all possible directions in the hemisphere of propagation by launching rays from its center; the initial amplitude and phase of a ray launched from the point $(x, y, 0)$ is

$$|U(x, y, 0)|e^{i\phi(x, y, 0)}$$

The phase of each ray changes as it moves; a ray that has travelled a distance d will have kd added to its phase where k is the wavenumber ($k = 2\pi/\lambda$ and λ is the wavelength). When a ray reaches the observation plane, it is added coherently to all others that have reached the same location.

2.2 Sampling

When sampling Huygen's wavelets is convenient to restrict the angles to those subtended by the detector (because other rays will miss the detector and not be recorded). Specifically, in the x - z plane, the angle that the new ray makes with the x -axis is

$$\theta_x = \theta_x^{\min} + \xi \cdot (\theta_x^{\max} - \theta_x^{\min})$$

where ξ is uniform random deviate between 0 and 1. The angle θ_x^{\min} is the smallest angle that reaches the detector from the starting location and θ_x^{\max} is the largest angle. A similar expression holds for θ_y . The direction cosines are

$$\mu = \left(\cos \theta_x, \cos \theta_y, \sqrt{1 - \cos^2 \theta_x - \cos^2 \theta_y} \right)$$

Restricting the angles creates a subtle bias because the subtended angles will differ in extent for different starting locations. This is corrected by weighting each ray by the subtended solid angle used to generate the launch angles. The correction for the amplitude (due to subtended angle) is

$$correction = (\theta_x^{\max} - \theta_x^{\min}) \cdot (\theta_y^{\max} - \theta_y^{\min})$$

It is efficient to sample how a flat coherent source field $U(x, y, 0) = 1$ propagates to the detector and to use this result to propagate all source field realizations. If N_s is the number of source elements and N_d is the number of detector elements, then this information can be recorded in a $N_s \times N_d$ matrix.* In the limit of an infinite number of infinitesimal source and detector elements, this mapping is functionally equivalent to a Green's function. For a finite number of elements the detector field can be written in terms of the Green's matrix G_{ij}

$$U_j = G_{ij}U_i$$

where the two-dimensional source field is represented as a vector U_i and the two-dimensional observation plane fields by U_j . The Monte Carlo is used to generate the values of G_{ij} by tracing rays from the i th source element to the j th detector element.

2.3 Diffraction by a Square Aperture

The stochastic simulation was validated by comparing with the expected intensity distribution for plane parallel light diffracted by a square aperture. The aperture width $a = 20\lambda$ and the detector was placed at a distance $d = 1000\lambda$ away. In the far-field limit, the Fraunhofer expression is

$$\frac{S(x, y, d)}{S(0, 0, d)} = \text{sinc}^2 \left(\frac{\pi ax}{\lambda \sqrt{d^2 + x^2}} \right) \text{sinc}^2 \left(\frac{\pi ay}{\lambda \sqrt{d^2 + y^2}} \right)$$

In the simulation the source has constant amplitude across each slit and is perfectly-coherent (so partial coherence is not tested). The source field is unity $U(x, y, 0) = 1$ within the aperture and zero elsewhere. For this simulation, the detector distance ($1,000\lambda$) is larger than $a^2/4\lambda = 100\lambda$ and the Fraunhofer approximation is appropriate.

*This linear list has a one-to-one mapping with the square grid of elements in the source and detector planes.

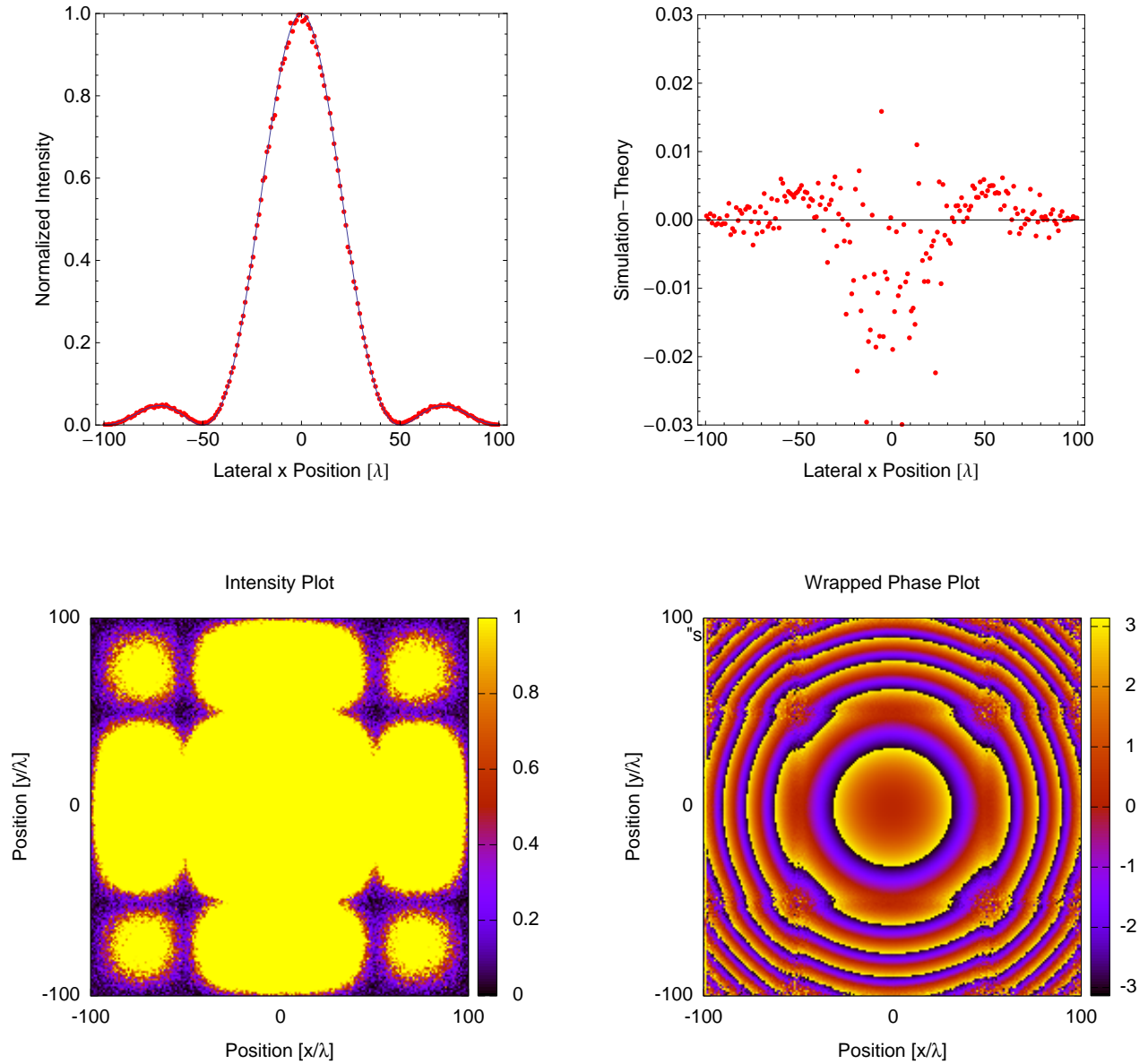


Figure 2. Normalized intensity $S(x, 0, 1000\lambda)/S(0, 0, 1000\lambda)$ on the detector. Solid line is the Fraunhofer approximation and the points are the simulation. The residuals are shown on the right. The source is a coherent flat field passing through a square aperture $20 \times 20\lambda$ in size to a detector 1000λ away. The detector has 200×200 pixels and is $200 \times 200\lambda$ in extent. The simulation used 10^9 rays.

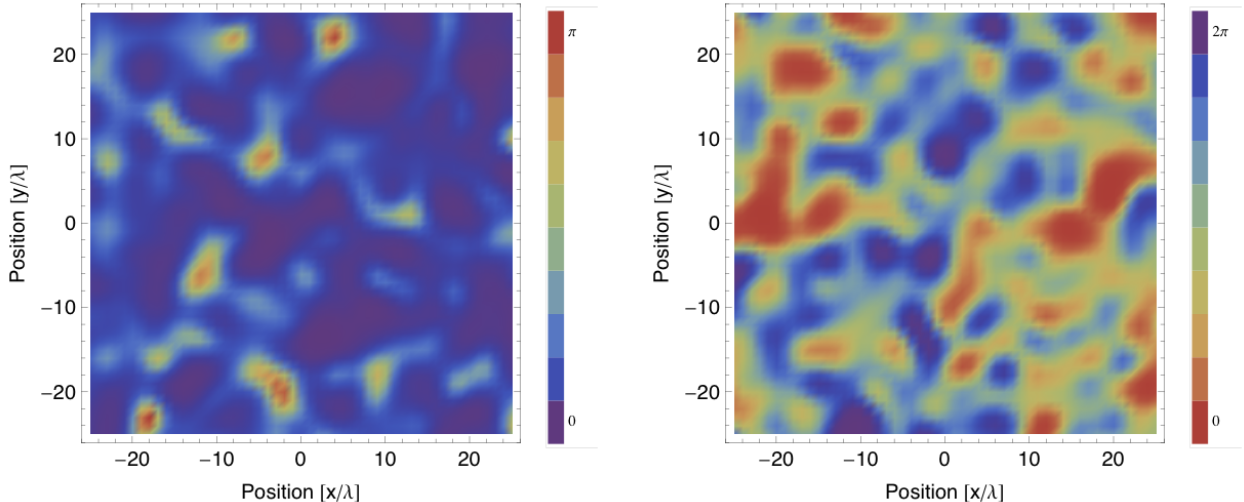


Figure 3. Random realizations of scattering angle (left) and azimuthal angle (right) for a Henyey-Greenstein phase function with $g = 0.9$. These realizations are 51×51 pixels in size. The colors for the azimuthal angle are evenly balanced because no angle is more likely than another. However, the scattering angle is strongly biased towards small angles because scattering is strongly forward directed.

3. SCATTERING BY A THIN LAYER OF TISSUE

Intensity measurements of the reflection and transmission of light as a function of angle allow direct measurement of the single-scattering phase function. The Henyey-Greenstein phase function has been found to be a good approximation to thin tissue scattering for skin⁷ and aorta.⁸ Consequently, if one wishes to simulate the propagation of coherence through tissue, then to get the first-order correlations (e.g., intensity) then the Henyey-Greenstein phase function is a suitable place to start.[†] The probability density function corresponding to the Henyey-Greenstein phase function is

$$p(\cos \theta) = \frac{1}{2} \frac{1 - g^2}{(1 + g^2 - 2g \cos \theta)^{3/2}}$$

The generating function for this distribution is

$$\cos \theta = \frac{1}{2g} \left\{ 1 + g^2 - \left(\frac{1 - g^2}{1 - g + 2g\xi} \right)^2 \right\}$$

where ξ is a uniformly distributed random deviate between 0 and 1. The azimuthal angle is distributed uniformly over $0-2\pi$ and is statistically independent of the scattering angle θ , thus

$$\phi = 2\pi\xi$$

3.1 Scattering Plate

We initially expected that traditional Gaussian phase plates could be used to model tissue scattering. Unfortunately, since propagation is a linear process if we start with a Gaussian process, we will end up with Gaussian scattering — not Henyey-Greenstein scattering. Consequently, we created a scattering plate¹⁰ by adapting a power spectral density technique.¹¹ Briefly, the Wiener-Khinchin theorem states that the correlation function Γ is related to the power spectral density S by a Fourier transform;

$$S = \mathcal{F}(\Gamma)$$

[†]Eventually, we will be using direct measurements of thin tissue samples using a differential interference contrast microscope.⁹

An array \mathbf{y} of Gaussian random samples with a prescribed local correlation may be generated using

$$\mathbf{y} = \text{Re}[\mathcal{F}^{-1}(e^{i2\pi\mathbf{u}}\mathbf{S}^{1/2})]$$

where \mathbf{u} is an $N \times N$ array of independent samples from a uniform distribution. Transformation of these Gaussian realizations via the cumulative distribution functions above for ϕ and $\cos\theta$ above yields an array of locally correlated distributed samples. We generated 51×51 pixel realizations that display a Gaussian autocorrelation function with a $1/e$ correlation length of 5 pixels and an asymmetry parameter $g = 0.9$.

3.2 Coherent Wave Propagation Through Scattering Plate

Two simulations with the phase plate in Figure 3 were performed. The first placed a plane of isotropic emitters directly behind the scatter plate. The second placed the source at $10,000\lambda$ behind the scatter plate. Rays were launched randomly from the source, as described above, and the intersection with the scatter plate ($51\lambda \times 51\lambda$) was found. This location determined the change θ in longitudinal angle and the change ϕ in the azimuthal angle. If (u, v, w) denotes the direction cosines of the incident ray, then the direction of the exiting ray (u', v', w') is

$$\left(u \cos \theta + \frac{uw \cos \phi - v \sin \phi}{\sqrt{1-w^2}} \sin \theta, v \cos \theta + \frac{vw \cos \phi + u \sin \phi}{\sqrt{1-w^2}} \sin \theta, w \cos \theta - \sqrt{1-w^2} \cos \phi \sin \theta \right)$$

as long as $|w| < 0.9$. Otherwise (u', v', w') is

$$\left(u \cos \theta + \frac{uv \cos \phi + w \sin \phi}{\sqrt{1-v^2}} \sin \theta, v \cos \theta - \sqrt{1-v^2} \cos \phi \sin \theta, w \cos \theta + \frac{vw \cos \phi - u \sin \phi}{\sqrt{1-v^2}} \sin \theta \right)$$

After hitting the scatter plate, the ray direction changed. The ray was propagated to the detector and the ray weight was added coherently to the appropriate detector bin. The results of two simulations are shown in Figure 4.

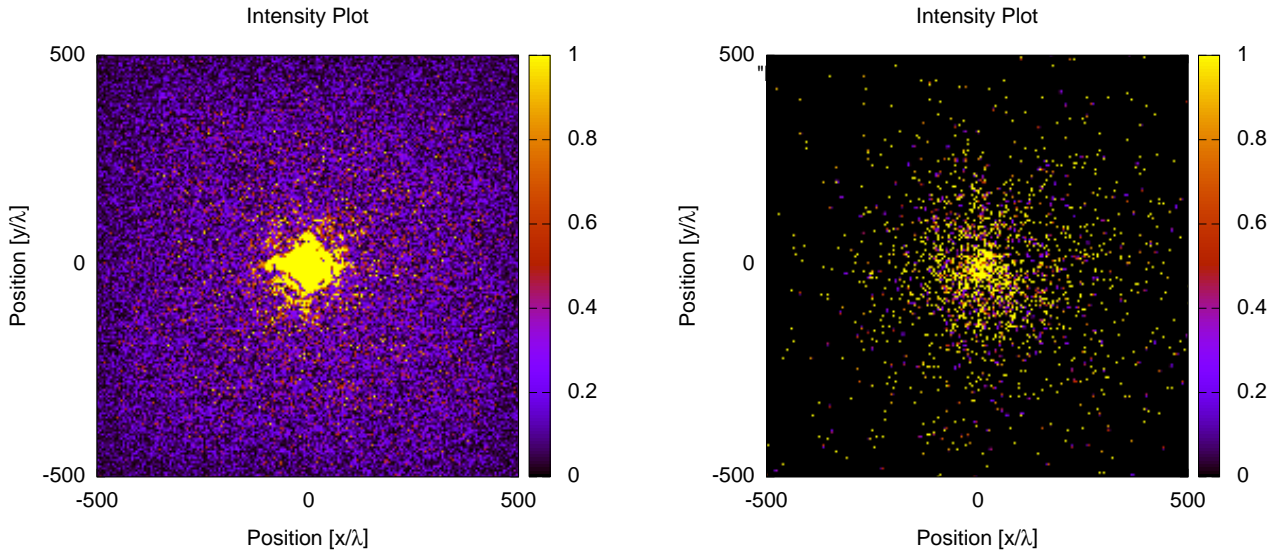


Figure 4. Normalized intensity at the detector $S(x, y, 0)/S(0, 0, 0)$ at a distance of $1,000\lambda$ from the scattering plate. The plot on the left shows the result when the source is directly behind the plate. The image on the right is the result when the source is located $10,000\lambda$ from the source. The detector has 200 pixels in each direction and is 1000λ wide. The calculations used 10^8 rays each.

REFERENCES

- [1] Fischer, D. G., Prahl, S. A. and Duncan, D. D., “Monte Carlo modeling of spatial coherence: free-space diffraction,” *J. Opt. Soc. Am. A* 25, 2571–2581 (2008).
- [2] Prahl, S. A., Duncan, D. D. and Fischer, D. G., “Monte Carlo propagation of spatial coherence,” in Wax, A. and Backman, V., eds., *SPIE Proceedings on Biomedical Applications of Light Scattering III*, volume 7187, 71870G–1–8 (2009).
- [3] Prahl, S. A., Fischer, D. G. and Duncan, D. D., “A Monte Carlo Green’s function for the propagation of partially coherent light,” *J. Opt. Soc. Am. A* 26, 1533–1543 (2009).
- [4] Duncan, D. D. and Kirkpatrick, S. J., “The copula: a tool for simulating dynamic speckle,” *J. Opt. Soc. Am. A* 25, 231–237 (2008).
- [5] Mandel, L. and Wolf, E., *Optical Coherence and Quantum Optics*, Cambridge University Press, Cambridge, UK (1995).
- [6] Goodman, J. W., *Statistical Optics*, Wiley (1985).
- [7] Jacques, S. L., Alter, C. A. and Prahl, S. A., “Angular dependence of HeNe laser light scattering by human dermis,” *Lasers Life Sci.* 1, 309–333 (1987).
- [8] Yoon, G., *Absorption and Scattering of Laser Light in Biological Media — Mathematical Modeling and Methods for Determining Optical Properties*, Ph.D. thesis, University of Texas at Austin (1988).
- [9] Duncan, D. D., Fischer, D. G., Daneshbod, M. and Prahl, S. A., “Differential interference contrast microscopy for the quantitative assessment of tissue organization,” in Conchello, J.-A., Cogswell, C. J., Wilson, T. and Brown, T. G., eds., *SPIE Proceedings on Three-Dimensional and Multidimensional Microscopy: Image Acquisition and Processing XVII*, volume 7570 (2010).
- [10] Duncan, D. D., Fischer, D. G., Daneshbod, M. and Prahl, S. A., “Tissue structural organization: measurement, interpretation, and modeling,” in Wax, A. and Backman, V., eds., *SPIE Proceedings on Dynamics and Fluctuations in Biomedical Photonics VII*, volume 7563 (2010).
- [11] Jakeman, E. and Ridley, K. D., *Modeling Fluctuations in Scattered Waves*, CRC Press, Boca Raton, FL (2006).